



Published in final edited form as:

Nature. 2020 September ; 585(7826): 569–573. doi:10.1038/s41586-020-2702-1.

The calcium-permeable channel OSCA1.3 regulates plant stomatal immunity

Kathrin Thor^{1,13}, Shushu Jiang^{1,7,13}, Erwan Michard², Jeffrey George^{1,3}, Sönke Scherzer⁴, Shouguang Huang⁴, Julian Dindas³, Paul Derbyshire¹, Nuno Leitão^{5,8}, Thomas A. DeFalco^{1,3}, Philipp Köster³, Kerri Hunter⁶, Sachie Kimura^{6,9}, Julien Gronnier^{1,3}, Lena Stransfeld^{1,3}, Yasuhiro Kadota^{1,10}, Christoph A. Bücherl^{1,11}, Myriam Charpentier⁵, Michael Wrzaczek⁶, Daniel MacLean¹, Giles E. D. Oldroyd^{5,12}, Frank L. H. Menke¹, M. Rob G. Roelfsema⁴, Rainer Hedrich⁴, José Feijó², Cyril Zipfel^{1,3,✉}

¹The Sainsbury Laboratory, University of East Anglia, Norwich Research Park, Norwich, UK.

²University of Maryland, Department of Cell Biology and Molecular Genetics, College Park, MD, USA.

³Institute of Plant and Microbial Biology, Zurich-Basel Plant Science Center, University of Zurich, Zurich, Switzerland.

⁴Department of Molecular Plant Physiology and Biophysics, University of Würzburg, Würzburg, Germany.

⁵Department of Cell and Developmental Biology, John Innes Centre, Norwich Research Park, Norwich, UK.

⁶Organismal and Evolutionary Biology Research Programme, Viikki Plant Science Centre, VIPS, Faculty of Biological and Environmental Sciences, University of Helsinki, Helsinki, Finland.

⁷Present address: Shanghai Institute of Biochemistry and Cell Biology, Center for Excellence in Molecular Cell Science, Chinese Academy of Sciences, Shanghai, China.

⁸Present address: Synthace Ltd, London, UK.

Reprints and permissions information is available at <http://www.nature.com/reprints>.

✉ Correspondence and requests for materials should be addressed to C.Z., cyril.zipfel@botinst.uzh.ch.

Author contributions C.Z. designed and supervised the project, and obtained funding. K.T. and S.J. conceived, designed and performed the majority of the plant and biochemical experiments. E.M. and J.F. provided the patch-clamp data in COS-7 cells; J. George performed some of the genetic and phenotypic characterization of the *osca1.3/1.7* mutant. P.D. and F.L.H.M. performed the SRM assays. N.L., M.C. and G.E.D.O. provided the yeast complementation assays. K.H. and M.W. provided the HEK cell data. T.A.D. and J.D. performed aequorin and YC3.6 measurements in leaf discs. P.K. and J. Gronnier generated expression constructs for OSCA1.7. L.S. assisted with the genetic characterization of the mutants. Y.K. provided initial data on the BIK1–OSCA1.3 interaction. C.A.B. provided OSCA1.3 localization data. S.S., S.H., M.R.G.R. and R.H. assisted with initial electrophysiological characterization, conducted ion flux measurements and carried out gas-exchange recordings. D.M. analysed the guard-cell Ca²⁺ measurements. K.T. and C.Z. wrote the manuscript. All authors commented and agreed on the manuscript before submission.

Online content

Any methods, additional references, Nature Research reporting summaries, source data, extended data, supplementary information, acknowledgements, peer review information; details of author contributions and competing interests; and statements of data and code availability are available at <https://doi.org/10.1038/s41586-020-2702-1>.

Competing interests The authors declare no competing interests.

Supplementary information is available for this paper at <https://doi.org/10.1038/s41586-020-2702-1>.

⁹Present address: Ritsumeikan Global Innovation Research Organization, Ritsumeikan University, Shiga, Japan.

¹⁰Present address: RIKEN Center for Sustainable Resource Science, Plant Immunity Research Group, Yokohama, Japan.

¹¹Present address: Dr. Friedrich Eberth Arzneimittel GmbH, Ursensollen, Germany.

¹²Present address: Sainsbury Laboratory Cambridge University, Cambridge, UK.

¹³These authors contributed equally: Kathrin Thor, Shushu Jiang.

Abstract

Perception of biotic and abiotic stresses often leads to stomatal closure in plants^{1,2}. Rapid influx of calcium ions (Ca^{2+}) across the plasma membrane has an important role in this response, but the identity of the Ca^{2+} channels involved has remained elusive^{3,4}. Here we report that the *Arabidopsis thaliana* Ca^{2+} -permeable channel OSCA1.3 controls stomatal closure during immune signalling. OSCA1.3 is rapidly phosphorylated upon perception of pathogen-associated molecular patterns (PAMPs). Biochemical and quantitative phosphoproteomics analyses reveal that the immune receptor-associated cytosolic kinase BIK1 interacts with and phosphorylates the N-terminal cytosolic loop of OSCA1.3 within minutes of treatment with the peptidic PAMP flg22, which is derived from bacterial flagellin. Genetic and electrophysiological data reveal that OSCA1.3 is permeable to Ca^{2+} , and that BIK1-mediated phosphorylation on its N terminus increases this channel activity. Notably, OSCA1.3 and its phosphorylation by BIK1 are critical for stomatal closure during immune signalling, and OSCA1.3 does not regulate stomatal closure upon perception of abscisic acid—a plant hormone associated with abiotic stresses. This study thus identifies a plant Ca^{2+} channel and its activation mechanisms underlying stomatal closure during immune signalling, and suggests specificity in Ca^{2+} influx mechanisms in response to different stresses.

Diverse environmental stimuli induce rapid increases in cytosolic Ca^{2+} concentrations ($[\text{Ca}^{2+}]_{\text{cyt}}$) to activate signalling responses⁵. In plants, rapid and transient $[\text{Ca}^{2+}]_{\text{cyt}}$ increases are, for example, triggered upon perception of PAMPs or abiotic stresses, such as hyper-osmolarity, drought or high ozone exposure^{6,7}. Leaf stomata, composed of two guard-cells, mediate water and gas exchanges and exhibit dynamic Ca^{2+} responses to stimuli. Stomata provide natural entry points for plant pathogens¹, and thus their closure must be tightly controlled to ensure optimal photosynthesis, while appropriately restricting evaporation and pathogen entry². Despite the central role of $[\text{Ca}^{2+}]_{\text{cyt}}$ for stomatal closure in response to multiple stimuli^{3,4}, the identities of the corresponding Ca^{2+} channels remain unknown.

In the model plant *A. thaliana* (hereafter, *Arabidopsis*), the plasma membrane-associated cytosolic kinase BIK1 and related PBL proteins act as central immune regulators downstream of multiple cell-surface immune receptors. BIK1 coordinates multiple immune outputs that are triggered by perception of PAMPs or damage-associated molecular patterns (DAMPs)^{8,9}. Previous work has shown that BIK1 directly phosphorylates the NADPH oxidase RBOHD to activate production of reactive oxygen species in response to perception

of PAMPs or DAMPs^{10,11}. Notably, BIK1 has been shown to be genetically involved in PAMP-induced Ca²⁺ influx and stomatal closure^{11–14}

We therefore hypothesized that BIK1 may directly phosphorylate one or more unknown Ca²⁺ channels involved in stomatal immunity. *Arabidopsis* OSCA1.3 (At1g11960), an uncharacterized isoform of the recently described OSCA/TMEM63 family of conserved Ca²⁺ channels^{15–19}, is rapidly phosphorylated upon PAMP treatment²⁰. Notably, two phosphopeptides in the predicted first cytoplasmic loop of OSCA1.3 contain a phosphorylated serine within a motif (Ser-X-X-Leu) that is conserved in RBOHD^{10,11} (Extended Data Fig. 1). *Arabidopsis* OSCA1.3 fused to green fluorescent protein (GFP) localizes to the plasma membrane (Extended Data Fig. 2), consistent with a possible role in mediating Ca²⁺ influx downstream of cell-surface immune receptors.

Next, we tested whether OSCA1.3 is a substrate of BIK1. Transiently expressed BIK1 fused to haemagglutinin (BIK1–HA) co-immunoprecipitated with OSCA1.3–GFP but not with the plasma membrane marker GFP–LTI6b (Fig. 1a). Treatment with the PAMP flg22—the ligand of the immune receptor FLS2 that activates BIK1^{21–23}—did not alter the association between OSCA1.3–GFP and BIK1–HA (Fig. 1a). BIK1–HA and OSCA1.3–GFP association was confirmed in transgenic *Arabidopsis* lines, but flg22 treatment reduced this association (Fig. 1b), in line with previous observations of the BIK1–RBOHD association^{10,11}.

We next sought to determine whether BIK1 phosphorylates OSCA1.3. The previously described OSCA1.3 phosphorylation sites²⁰ are located in the first cytoplasmic loop (loop1; Extended Data Fig. 1). In vitro pull down and radioactive kinase assays showed that OSCA1.3-loop1 directly interacts with, and can be phosphorylated by glutathione *S*-transferase (GST)–BIK1 (Fig. 2a, b). This phosphorylation is dependent on BIK1 kinase activity, since a kinase-dead variant, GST–BIK1(KD), did not phosphorylate OSCA1.3-loop1 fused to maltose binding protein (MBP) (Fig. 2b). Targeted mutagenesis of the identified phosphorylation sites (S49 and S54) and the adjacent S50 in OSCA1.3-loop1 (Extended Data Fig. 1) followed by in vitro radioactive kinase assays showed that BIK1 predominantly phosphorylates S54 (Fig. 2b). Consistent with a partially-overlapping role with BIK1^{10–13,22}, the phylogenetically-related PBL1 kinase could also specifically phosphorylate OSCA1.3-loop1 at S54 (Extended Data Fig. 3). Notably, flg22-induced BIK1-dependent phosphorylation on S54 was confirmed in vivo using selected-reaction monitoring (SRM) assays (Fig. 2c), further demonstrating that OSCA1.3 is a substrate of BIK1 during immune signalling.

There are 15 OSCA isoforms in *Arabidopsis*, which are grouped in 4 different phylogenetic clades^{15,24}. Of these, only OSCA1.1 and OSCA1.2 (also known as CSC1) have been functionally characterized in planta, and are involved in response to osmotic stress^{15,16}. Other OSCA isoforms in *Arabidopsis* and rice (*Oryza sativa*) have been recently shown to be mechanosensitive non-selective cation channels and, in some cases, are proposed to be Ca²⁺-permeable^{24–28}. To test whether OSCA1.3 is a Ca²⁺-permeable channel, we first made use of the Ca²⁺-uptake deficient yeast mutant *cch1/mid1*²⁹. This mutant did not grow in a halo around a filter paper disc soaked in mating pheromone α factor, compared with wild-type yeast or the *cch1/mid1* mutant expressing OSCA1.3 (Fig. 3a), suggesting

that OSCA1.3 facilitates Ca^{2+} transport in this heterologous system. Expression of myc-tagged OSCA1.3 in human embryonic kidney 293T (HEK293T) cells and measurements using the Ca^{2+} -sensitive ratiometric fluorescent dye Fura-2 further indicated that OSCA1.3 expression can lead to increases in $[\text{Ca}^{2+}]_{\text{cyt}}$ (Extended Data Fig. 4). Finally, patch-clamp recordings with COS-7 cells revealed currents upon expression of OSCA1.3, which were increased upon BIK1 co-expression in a kinase-activity-dependent and OSCA1.3-S54 phosphorylation-dependent manner (Fig. 3b, c, Extended Data Fig. 5a). Together, these results show that OSCA1.3 is a BIK1-activated Ca^{2+} -permeable channel.

Within OSCA clade 1 in *Arabidopsis*, only OSCA1.7 (At4g02900) has a Ser-X-X-Leu motif similar to that of OSCA1.3 at the same position (Extended Data Fig. 1b). Consistently, OSCA1.7-mediated currents in COS-7 cells were activated by BIK1 activity (Extended Data Fig. 5b, c). Notably, OSCA1.3 and OSCA1.7 alone were permeable to Ca^{2+} and this activity was not increased upon co-expression of both channels (Fig. 3b, c, Extended Data Fig. 5b, c). We generated a double homozygous insertional *osca1.3/osca1.7* (hereafter *osca1.3/1.7*) null mutant (Extended Data Fig. 6a, b, Extended Data Fig. 7). The overall increase of $[\text{Ca}^{2+}]_{\text{cyt}}$ in response to flg22 treatment in leaf discs of transgenic wild-type (Col-0) or *osca1.3/1.7* lines expressing the cytosolic Ca^{2+} sensor aequorin^{12,30} was similar (Extended Data Fig. 8a). As *OSCA1.3* is preferentially expressed in guard cells (Extended Data Fig. 7) and BIK1 controls several aspects of stomatal immunity^{10,11,22}, we generated transgenic lines in wild-type (Col-0) or *osca1.3/1.7* backgrounds expressing the cytosolic ratiometric Ca^{2+} sensor YC3.6, which enables measurement of flg22-induced Ca^{2+} spiking with cellular resolution³¹. Single-cell measurement of Ca^{2+} spiking in guard cells showed that the rapid (5-min) flg22-induced Ca^{2+} increase was reduced in *osca1.3/1.7* compared to Col-0 (Fig. 4a, Extended Data Fig. 9a). A similar reduction was observed using non-invasive microelectrode ion flux measurements (Extended Data Fig. 9b, c). Consistent with data from the aequorin reporter line (Extended Data Fig. 8a), no such decrease was observed in leaf discs of the *osca1.3/1.7*YC3.6 line (Extended Data Fig. 8b), suggesting that the *osca1.3/1.7* defects are specific to guard cells.

Unexpectedly, we observed that the quantitatively dampened increase of flg22-induced $[\text{Ca}^{2+}]_{\text{cyt}}$ in guard cells correlated with an abolishment of flg22-induced stomatal closure in *osca1.3/1.7* (Fig. 4b). Notably, stomatal closure in *osca1.3/1.7* was similarly impaired upon treatment with the DAMP AtPep1 (Fig. 4c). However, stomatal closure in response to the plant stress hormone abscisic acid (ABA) was not affected in *osca1.3/1.7* (Fig. 4c), corroborated by stomatal conductance measurements in intact leaves (Fig. 4d, Extended Data Fig. 10). These results reveal that loss of OSCA1.3 and OSCA1.7 does not generally affect guard cell physiology, suggesting that OSCA1.3 and OSCA1.7 have a specific role in stomatal closure during immunity. Consistently, *osca1.3/1.7* plants were more susceptible than wild-type (Col-0) to the hypovirulent *Pseudomonas syringae* pv. tomato DC3000 *COR* strain to a level comparable with the immune-deficient mutant *bak1-5* (Fig. 4e).

Finally, to test whether the role of OSCA1.3/1.7 depends on BIK1-mediated phosphorylation, we complemented *osca1.3/1.7* with either *OSCA1.3* or *OSCA1.3^{S54A}*. Expression of OSCA1.3, but not OSCA1.3(S54A) restored flg22-induced stomatal closure (Fig. 4f). In sum, our data demonstrate that OSCA1.3 is a Ca^{2+} -permeable channel required

for stomatal immunity, the activation and function of which depend on BIK1-mediated phosphorylation.

It is noteworthy that the quantitative reduction of Ca^{2+} influx observed in single guard cells leads to a complete abolishment of elicitor-induced stomatal closure. Thus, our work identifies an elusive Ca^{2+} channel involved in early immune signalling, indicative of a threshold mechanism for the regulation of this important adaptive stress response. We cannot however completely exclude that OSCA1.3 or OSCA1.7 might be permeable to additional cations that may also contribute to stomatal closure, as other OSCAs have been shown to be non-selective cation channels^{24–28}. Notably, neither OSCA1.3 or OSCA1.7, nor their regulation by BIK1 appears to be required for ABA-induced stomatal closure. These results further support that PAMPs and ABA activate components leading to stomatal closure through independent mechanisms^{32,33}. Moreover, our study reveals a critical activation mechanism for this channel via phosphorylation by BIK1. Several plant OSCAs have recently been shown to be mechanosensitive Ca^{2+} channels^{24–28}. It remains to be tested whether OSCA1.3 and OSCA1.7 are similarly mechanosensitive, but our results suggest that phosphorylation by plasma membrane-associated kinases could represent an additional layer of regulation for this conserved family of Ca^{2+} channels in response to distinct stimuli, as recently shown for cyclic nucleotide-gated channels in the context of mesophyll immunity^{14,34}. Further work is needed to understand how BIK1 and OSCAs—together with additional isoforms from other Ca^{2+} channel families proposed to be involved in immunity^{14,34–38}—help integrate calcium signalling at the plant tissue and organ scales.

Methods

No statistical methods were used to predetermine sample size. The experiments were not randomized and investigators were not blinded to allocation during experiments and outcome assessment.

Plant material and growth conditions

All *A. thaliana* lines used in this study were in the Col-0 ecotype background. Lines *osca1.3* (SALK_134381) and *osca1.7* (SALK_114694) were obtained from the Nottingham *Arabidopsis* Stock Centre (NASC) and genotyped for homozygosity using left border and gene-specific primers listed in Supplementary Table 2. Line *osca1.3/1.7* was obtained by crossing *osca1.3* and *osca1.7* and screening the F₂ for double homozygous progeny. *bak1–5* has been described previously³⁹. Unless stated otherwise, plants were grown on soil as one plant per pot with a 10-h photoperiod at 20 to 22 °C in environmentally controlled growth rooms. Four-to-five-week-old plants were used for experiments unless stated otherwise. Col-0 plants stably expressing Yellow Cameleon 3.6 under the *ubiquitin10* promoter were kindly provided by M.C. Mutant plants were crossed with this line and progeny screened for homozygosity of the T-DNA insertions and the presence of the YC3.6 reporter. Lines expressing the calcium reporter aequorin under the control of the 35S promoter were generated by transforming Col-0, *osca1.3*, *osca1.7* and *osca1.3/1.7* with the construct pB7WG2:aequorin via agrobacterium-mediated transformation. Selection of transformants was performed on BASTA-containing full strength MS medium and transformants were

screened for similar aequorin levels in the T1 generation via western blot with aequorin antibody (Abcam ab9096). T2 plants were used for assays. Complementation lines were generated by transforming *osca1.3/1.7* plants with pGWB1-pOSCA1.3:OSCA1.3(WT) or pGWB1-pOSCA1.3:OSCA1.3(S54A) by agrobacterium-mediated transformation. T1 plants were selected on hygromycin-containing MS medium supplemented with 1% sucrose and directly used for stomatal aperture assays. Col-0 and *osca1.3/1.7* plants were grown in parallel under the same conditions on non-selective medium. Expression levels for *OSCA1.3* were checked using quantitative PCR with reverse transcription (RT-qPCR) to document complementation (Extended Data Fig. 6c). Double transgenic lines were generated by crossing the *pBIK:BIK1-HA* line^{10,22} with the *p35S:GFP-LTI6b* line⁴⁰ or transforming *pBIK:BIK1-HA* plants with construct p35S:OSCA1.3-GFP by *Agrobacterium*-mediated transformation.

Chemicals

Synthetic flg22 and AtPep1 were purchased from EZBiolab and dissolved in sterile water. ABA was purchased from Sigma-Aldrich.

Homology modelling for OSCA1.3

SWISS-MODEL⁴¹ and HHPRED⁴² were used to search for structural homologues to full length OSCA1.3. The structural modelling of OSCA1.3 was performed using SWISS-MODEL⁴¹ with OSCA1.2 (PDB-ID: 6MGV)²⁶ as template. Images were created with CHIMERA⁴³.

Molecular cloning

For OSCA1.3 subcellular localization detection in *Arabidopsis*, the fragment of the promoter region (1,226 bp) and the coding region of *OSCA1.3* genomic DNA was amplified and inserted into the Entry vector pCR8 (Invitrogen) by TOPO-TA cloning, and then introduced into the Gateway binary vector pGWB4 with a GFP tag at the C terminus after recombination by LR Clonase II (Invitrogen). For protein expression in *N. benthamiana*, we generated epiGreenB-p35S:OSCA1.3-GFP by inserting the *OSCA1.3* cDNA fragment into epiGreenB (eGFP) vector using the In-fusion enzyme (Clontech Laboratories), and used previous reported pGWB14-p35S:BIK1-3 × HA (ref.⁴⁴) as well as p35S:GFP-LTI6b (ref.⁴⁰) constructs. Site-directed mutagenesis of *OSCA1.3* was achieved by PCR using overlapping primers containing the desired point mutations. To generate constructs for *Arabidopsis* complementation assay, *pOSCA1.3:OSCA1.3(WT)* and *pOSCA1.3:OSCA1.3(S54A)* were cloned into Entry vector pCR8 and then introduced into gateway binary vector pGWB1 with no epitope tag⁴⁵. For protein expression in *Escherichia coli*, *OSCA1.3* (88–285 bp) and its mutant variants were cloned into pOPINM vector using in-fusion enzyme to generate an N-terminal 6×His-MBP fusion. GST-BIK1 and GST-BIK1(KD) constructs have been described previously²³. GST-PBL1 and GST-PBL1(KD) fusions were created after recombination using respective entry clones and gateway vector pABD72_pGEX-2TMGW. For expression in COS-7 cells, coding sequences of OSCA1.3, OSCA1.3(S54A), BIK1 and BIK1(KD) (BIK1(K105A/K106A))⁴⁴ were PCR-amplified with primers listed in Supplementary Table 2 and cloned into the vector pCI (Promega) by restriction enzyme cloning. The coding sequence of OSCA1.7 was synthesized with the corresponding

restriction sites and subcloned into pCI. For expression in yeast, the *OSCA1.3* coding sequence was converted to yeast codon usage using Geneious 8.1.8, synthesized by Life Technologies (ThermoFisher Scientific) into the entry vector pENTR221 and subsequently cloned into the destination vector pYES-DEST52 with Gateway LR Clonase II Enzyme Mix (Invitrogen).

Protein expression and purification

For protein purification, constructs were transformed into the *E. coli* expression strain BL21 (DE3). The bacterial culture was grown to an OD₆₀₀ of 0.6, and 0.5 mM IPTG was then added to induce protein expression. The induction continued at 16 °C overnight. His-MBP-OSCA1.3 variants were purified using nickel resin with buffer A (50 mM Tris-HCl, pH 8.0, 500 mM NaCl, 5% glycerol and 20 mM imidazole) containing 0.5 mM DTT and 0.2 mM PMSF as lysis buffer. Purified proteins were eluted in buffer B (50 mM Tris-HCl, pH 8.0, 500 mM NaCl, 5% glycerol, and 200 mM imidazole) after 5 washes using buffer A. GST-BIK1 or GST-PBL1 was purified using glutathione resin. Buffer C (20 mM Tris-HCl, pH 7.5, and 500 mM NaCl) with 0.5 mM DTT and 0.2 mM PMSF was used as lysis buffer and buffer D (20 mM Tris-HCl, 500 mM NaCl and 20 mM reduced glutathione, pH adjusted to 7.0) was used as elution buffer. After purification, all proteins were dialysed into buffer E (20 mM Tris-HCl, pH7.5, 150 mM NaCl and 5 mM DTT) for further application.

Co-immunoprecipitation in *N. benthamiana*

Two leaves of 4- to 5-week-old *N. benthamiana* plants were syringe-infiltrated with *Agrobacterium tumefaciens* strain GV3101 expressing GFP-OSCA1.3 and BIK1-HA. Two days later, leaves were cut and halves treated with either 1 µM flg22 or mock for 10 min. The tissue was ground in liquid nitrogen and homogenized in extraction buffer (0.5% (w/v) PVPP, 150 mM Tris-HCl, pH 7.5, 150 mM NaCl, 10% glycerol, 10 mM EDTA, 1 mM NaF, 1mM NaMo, 1.5 mM Na₃VO₄, 10 mM DTT, 1% protease inhibitor cocktail (Sigma Aldrich) and 1 mM PMSF) with 1% Igepal CA-630. The supernatant obtained after centrifugation was incubated with 25 µl of GFP-Trap agarose beads (ChromoTek). Following an incubation for several hours at 4 °C, the beads were washed 3 times using extraction buffer with 0.5% Igepal CA-630 before SDS-PAGE and western blot detection with GFP antibody (Santa Cruz, 1:5,000) and haemagglutinin antibody (Roche, 1:2,000). For blot source data, see Supplementary Fig. 1.

Co-immunoprecipitation in *Arabidopsis*

Sterilized seeds were sown on MS agar plates. After stratification for 3 days in the dark at 4 °C, seeds were transferred to light. Four days later, ten seedlings were transferred into each well of a 6-well plate containing liquid MS. Two-week-old seedlings from two 6-well plates were elicited by 1 µM flg22 for 10 min. MS medium treatment was used as a control. Tissue was ground in liquid nitrogen and extraction buffer (150 mM Tris-HCl, pH 7.5, 150 mM NaCl, 10% glycerol, 5 mM EDTA, 10 mM NaF, 10 mM NaMo, 2 mM Na₃VO₄, 5 mM DTT, 1× protease inhibitor cocktail 1, 1× protein phosphatase inhibitor cocktail 2 (Sigma Aldrich), and 1 mM PMSF) containing 2% IGEPAL CA-630 was added to the resulting powder at 2 ml g⁻¹ tissue. After homogenizing for 1 h, samples were centrifuged for 20 min at 13,000 rpm at 4 °C. The concentration of IGEPAL CA-630 in the supernatant was adjusted to

0.5% by diluting the samples with extraction buffer. For immunoprecipitation, 100 μ l of GFP agarose beads (Chromotek) were added. After incubation for 2 h, beads were washed 3 times using extraction buffer containing 0.5% IGEPAL CA-630 before SDS-PAGE and western blot detection with GFP (Santa Cruz, 1:5,000) and haemagglutinin (Roche, 1:2,000) antibodies. For gel and blot source data, see Supplementary Fig. 1.

In vitro GST pull down

Glutathione resin Sepharose 4 Fast Flow (GE Healthcare) was equilibrated with incubation buffer (20 mM Tris-HCl, pH 7.5, 50 mM KCl, 5 mM MgCl₂, 1% Tween 20, 1 mM DTT and 100 μ M PMSF). Ten micrograms of the GST fusion proteins were incubated with the resin in incubation buffer for 2 h. Subsequently, the resin was washed 3 times with incubation buffer before the second incubation with 10 μ g of MBP fusion proteins. After 1 h incubation, the resin was washed 5 times and boiled in 6 \times SDS loading buffer for SDS-PAGE and western blot detection with GST (Sigma-Aldrich, 1:1,000), rabbit IgG (Sigma, 1:10,000) and MBP (New England Biolabs, 1:5,000) antibodies. For blot source data, see Supplementary Fig. 1.

In vitro kinase assay

One microgram of kinase and substrate were mixed up to 20 μ l in buffer containing 50 mM Tris-HCl, pH 7.5 and 3 mM MnCl₂. Five microlitres of 5 \times kinase buffer (25 mM MnCl₂, 5 mM DTT and 5 μ M unlabelled ATP) was added to each reaction. Every reaction was incubated with 183 KBq of [³²P]- γ -ATP for 30 min at 30 °C while shaking. Reactions were stopped by adding 6 \times SDS loading buffer. After SDS-PAGE separation, proteins were transferred onto PVDF membranes followed by staining with CBB. Phosphorylation of proteins was detected by autoradiography using a FUJI Film FLA5000 PhosphorImager (Fuji, Tokyo). For blot source data, see Supplementary Fig. 1.

Confocal laser scanning microscopy

Cotyledons of *Arabidopsis* seedlings were imaged on a Leica TCS SP5 (Leica, Germany) confocal microscope using a 63 \times 1.2 NA water immersion objective. GFP was excited using the Argon ion laser line 488 nm. Fluorescence emission was collected within following band width generated by an AOTF: 500–540 nm for GFP. Confocal micrographs were analysed and modified using FIJI (ImageJ 2.0.0–39/rc-1.50b).

Seedling growth and elicitation with flg22 for SRM

Approximately 20 mg of sterilised seeds were sown into a 250 ml sterile conical flask containing 50 ml liquid medium (1/2 MS salts, 1% (w/v) sucrose, pH 5.7), sealed with foil wrapping and chilled for 48 h, 4 °C in darkness. Flasks were transferred to an orbital shaker (New Brunswick Innova 2300) rotating at 140 rpm in a 16 h light:8 h dark photoperiod at 21 °C. After 7 d, the seedling clumps were vacuum infiltrated with 1 μ M flg22 peptide for 1 min with shaking before releasing to atmospheric pressure. Excess liquid was removed from the clumps and clumps were frozen in liquid nitrogen after 5 min exposure to flg22. Untreated (t₀) controls were only vacuum infiltrated before drying and freezing.

Protein extraction and trypsin digestion for SRM

Frozen seedling clumps were ground to a coarse powder in liquid nitrogen and further disrupted using a Braun 853202 homogenizer (B. Braun Melsungen AG) at 1,200 rpm for 5 min with a Potter–Elvehjem glass pestle in a 30 ml glass tube (Sartorius) containing 10 ml ice-cold kinase extraction buffer (50 mM Tris pH7.5, 10% glycerol, 2 mM DTT, 10 mM NaF, 10 mM Na₂V₀₄, 5 mM EDTA, 50 mM β-glycero-phosphate, 1 mM PMSF and 100 μl protease inhibitor cocktail (Sigma)) surrounded with an ice jacket. Crude extracts were centrifuged at 4,300g for 1 h at 4 °C to remove cell debris followed by ultracentrifugation at 100,000 g for 30 min at 4 °C to create a microsome-enriched pellet. After removal of supernatant the pellet was solubilized in 8 M urea/50 mM ammonium bicarbonate to denature proteins.

Up to 3 mg protein was reduced with 5 mM tris(2-carboxyethyl)phosphine 20 min, 37 °C, 200 rpm then alkylated with 40 mM iodoacetamide, for 60 min at 25 °C, under shaking at 200 rpm. Samples were diluted in 5 volumes 50 mM ammonium bicarbonate to reduce urea concentration. Sequencing grade trypsin (Thermo) was added at 1:100 (w/w) enzyme:substrate and incubated for 16 h and 37 °C and 200 rpm. The reaction was stopped by acidification with 1% (v/v) trifluoroacetic acid. Peptides were cleaned-up using C18 silica reversed-phase chromatography columns (Sep-Pak) according to the manufacturer's instructions and the final eluates dehydrated in an acid resistant speed-vac.

Phosphopeptide enrichment for SRM

Lyophilized tryptic peptides were resuspended by sonication in phthalic acid/80% acetonitrile (0.1 g ml⁻¹) solution which had been further acidified with 3.6% (v/v) trifluoroacetic acid. The peptide solution was loaded into a Mobicol spin column containing 1.56 mg TiO₂-coated particles (Titanosphere) that had been previously washed in MeOH and equilibrated in phthalic acid/acetonitrile solution (above). The sealed columns containing the peptide/TiO₂ solution were incubated for 45 min on a head-over-tail rotor followed by washes in phthalic acid/acetonitrile solution, 80% (v/v) acetonitrile/0.1% trifluoroacetic acid, 0.1% (v/v) trifluoroacetic acid. Peptides were eluted with NH₄OH solution (pH 10.5) into a sufficient amount (usually 60–80 μl of 10% (v/v) trifluoroacetic acid to give a final pH of 2–3. The enriched phosphopeptide solution was cleaned using C18 MicroSpin Columns (The Nest Group Inc.) and eluted into low-bind microfuge tubes with 40% (v/v) acetonitrile.

Identification of proteins and phosphopeptides by LC–MS/MS for SRM

Liquid chromatography with mass spectrometry (LC–MS/MS) analysis was performed using a Fusion–Orbitrap mass spectrometer (Thermo Scientific) and a U-3000 nanoflow-HPLC system (Thermo Scientific) as described previously⁴⁶. The entire TAIR10 database was searched (www.Arabidopsis.org) using Mascot (v.2.3.02, Matrix Science) (with the inclusion of sequences of common contaminants, such as keratins and trypsin). Parameters were set for 10 ppm peptide mass tolerance and allowing for Met oxidation and two missed tryptic cleavages. Carbamidomethylation of Cys residues was specified as a fixed modification, and oxidation of Met and phosphorylation of Ser, Tyr or Thr residues were allowed as variable modifications. Scaffold (v.3; Proteome Software) was used to validate

MS/MS-based peptide and protein identifications and annotate spectra. The position and quality of spectra for phosphopeptides were also manually examined before acceptance.

SRM analysis and relative quantification of phosphorylation

Synthetic peptides (JPT Peptide Technologies) for OSCA1.3 Psspl-HSGALVSK, SpSPLHSGALVSK and SSPLHpSGALVSK were used to optimise an SRM method for detection in the phosphopeptide enriched samples using the program Skyline⁴⁷. Control peptides used for normalization were selected from an initial shortlist of 30 on the basis of their spectral counts in each sample not deviating $\pm 25\%$ from the median value of all samples. An SRM method was designed to measure these peptides with better resolution but this time to confirm that the average intensity in each sample did not deviate ± 1 s.d. from the mean intensity of all samples. Retention times and transitions were confirmed by targeting the control peptides in a ¹⁵N-labelled phosphopeptide mix derived from total *Arabidopsis* protein. Eight control peptides with a similar dynamic range were selected for normalization and incorporated into the SRM method containing the SSPLHSGALVSK phosphopeptide variants given in Supplementary Table 1. iRTs (Biognosys) were added to each injection to track and correct for retention time changes. Peptide sequence, precursor *m/z* and transitions are specified in Supplementary Table 1.

SRM analysis was performed using nano-spray ESI and a TQ-S MS (Waters). The liquid chromatography system consisted of a nanoAcquity with a Symmetry trap (Waters, C18, 180 $\mu\text{m} \times 20$ mm) to concentrate and desalt the peptides before elution to the analytical column (Waters, CSH 250 mm C18 columns, 75 μm internal diameter, 1.7 μm beads). A flow rate of 250 nl min^{-1} was used with a gradient from 3% to 65% acetonitrile over 90 min. One or two injections were performed from one to three independent biological replicates. The resultant TQ-S files were imported into Skyline and the peak definitions checked manually. The peak areas were then exported into Excel (Microsoft) for further analysis. The summed intensity of each OSCA1.3 phosphopeptide was normalized (by division) against the summed intensities of the eight control peptides for relative quantification. All SRM assay information and raw data have been deposited to the Panorama Skyline server and can be accessed via <https://panoramaweb.org/Vzao3P.url>.

Yeast complementation

Yeast complementation was performed as described⁴⁸. In brief, the *cch1/mid1* mutant⁴⁹ was transformed via the lithium acetate method⁵⁰ with either the vector pYES-DEST52 (Invitrogen) expressing Ds-Red or pYES-DEST52 expressing OSCA1.3 (codon bias corrected for yeast expression) and transformants selected on yeast minimal medium without uracil. To test for complementation, sterile cellulose filter discs (6 mm diameter and 45 μm pore size) were soaked with 10 μg synthetic alpha factor (Sigma T6901) and placed on nascent lawns of WT (JK9-3da (*MAT α* , *leu2-3*, *112*, *his4*, *trp1*, *ura3-52*, *rme1*)) or the transformed *cch1/mid1* mutants and pictures taken after 48 h of growth at 30 °C.

COS-7 cell transfection and patch-clamp

COS-7 cells (ATCC) were used at low passage ($P < 7$). They were maintained at 37 °C and 5% CO_2 in Dulbecco's Modified Eagle's Medium, supplemented with 5% fetal

bovine serum and 1% penicillin/streptomycin (Gibco, Thermofisher). The coding sequences of OSCA1.3, OSCA1.3(S54A), OSCA1.7, BIK1 and BIK1(KD) were introduced into pCI (Promega). COS cells were plated at a density at 50% confluence in 35-mm-diameter dishes and transfected using FugeneHD (Promega) as specified by the supplier. Cells were transfected with pCI-OSCA1.3 (0.4 μg), pCI-OSCA1.3(S54A) (0.4 μg), pCI-OSCA1.7 (0.4 μg) or pCI-OSCA1.3 (0.2 μg) plus pCI-OSCA1.7 (0.2 μg), with pCI-BIK1 (0.4 μg), pCI-BIK1(KD) (0.4 μg) or pCI (0.4 μg). PIRES-CD8 (0.05 μg) was co-transfected to select expressing cells⁵¹. Cells were transferred in new Petri dishes 36 h after transfection (by trypsin treatment), at low density for patch-clamp study. Cells were analysed 36 to 40 h after transfection. Transfected cells were detected with the CD8 antibody-coated bead method (Dynabeads CD8, Thermofisher)⁵². Pipettes were pulled with a P97 puller (Sutter Instrument). Their resistance was: 3–5 M Ω . Currents were recorded after establishing the whole-cell configuration⁵³, filtered at 1–2 kHz with a sampling frequency of 2–4 kHz using an Axopatch 200A amplifier, Digidata 1200 series interface and Clamfit6 software (Molecular device). Except for Extended Data Fig. 5a, the pipette solution contained 140 mM Na-gluconate, 3 mM MgCl₂, 4 mM HCl, 5 mM EGTA, and 10 mM Bis-tris propane pH 7.2 (Hepes). Except for Extended Data Fig. 5a, the bath solution contained 10 mM Na-gluconate, 20 mM Ca-gluconate, and 10 mM Bis-Tris propane, pH 6.5 (MES). Extended Data Fig. 5a pipette solution: MgCl₂ 3 mM, EGTA 5 mM, HCl 4 mM, Bis-Tris propane pH 7.2 (Hepes). Extended Data Fig. 5a bath solution: CaCl₂ 5mM, Bis-Tris propane pH 6.5 (MES). Ca-gluconate was added to the standard bath solution to increase external calcium concentration to 25, 45 and 65 mM successively. The junction potentials of the different solutions in Extended Data Fig. 5a were calculated using pClamp6 software and corrected accordingly. Solutions were adjusted to 350 mOsmol kg⁻¹ with D-mannitol. Voltage protocol: 1.5-s pulses from –100 to +60 mV (20-mV steps), holding potential 0 mV.

Calcium measurements in HEK cells

HEK293T cells (ATCC, CRL-3216) were maintained at 37 °C and 5% CO₂ in Dulbecco's Modified Eagle's Medium F12-HAM (Sigma-Aldrich), supplemented with 10% fetal bovine serum, 15 mM HEPES, and 1% penicillin/streptomycin. For calcium experiments, cells were seeded on black, clear-bottom, half-volume 96-well plates coated with polyethylenimine (25 $\mu\text{g ml}^{-1}$ for 1 h at 37 °C; Sigma-Aldrich). Cells were transiently transfected using GeneJuice (Novagen) according to the manufacturer's instructions.

Calcium measurements were performed 40 h after transfection. Cells were loaded for 1 h at 37 °C with a 1:1 mixture of Fura-2-QBT calcium kit (Molecular Devices) and calcium-free NaE buffer (137 mM NaCl, 5 mM KCl, 1.2 mM MgCl₂, 4.2 mM NaHCO₃, 0.44 mM KH₂PO₄, 20 mM HEPES, adjusted to pH 7.4 with NaOH), plus 10 mM glucose and 2 mM probenecid. Intracellular Ca²⁺ was assessed by measuring changes in fluorescence with a FlexStation 3 fluorescence plate reader (Molecular Devices) at 37 °C. Measurements were recorded at 340/510 nm and 380/510 nm (excitation/emission) every 6 s for a total of 530 s. Additions of sorbitol were made at 30 s (final concentration 1.3 M) and CaCl₂ at 150 s (final concentration 0.6 mM). Data were presented as the ratio of the 340/380 measurements and were normalized to the baseline before additions.

Calcium measurements in aequorin lines

Twelve leaf discs per line from 6 individual plants were incubated in a 12.5 μM coelenterazine h (Cayman Chemical) solution overnight to reconstitute aequorin. The next day, the coelenterazine solution was replaced by water and luminescence measured in a Synergy H1 plate reader (BioTek) with a measuring time of 40 ms and a 30-s interval. After 10 min, flg22 was added to a final concentration of 100 nM and measurement was continued for another 45 min before discharging with a calcium chloride/ethanol solution to a final concentration of 1M/10%. Discharging values were measured for 99 s. Background luminescence was subtracted and cytosolic calcium concentrations were calculated as previously described⁵⁴.

Calcium measurements in leaf disc of YC3.6 lines

Leaf discs (4 mm in diameter) of 3- to 5-week-old *A. thaliana* plants were collected with a biopsy punch and dark incubated at room temperature overnight in a 96-well plate in 0.1 ml deionized water with the abaxial site up. Fluorescence measurements were carried out in a Synergy H1 hybrid plate reader (BioTek Instruments) equipped with a Xenon flash lamp. In 45-s intervals CFP was excited at 440 nm and emission signals were detected at 480 nm (CFP) and 530 nm (YFP). Flg22 was added to a final concentration of 1 μM through a built-in dispenser system. For quantification of the signal, YFP emission at CFP excitation was divided by CFP emission at CFP excitation.

Calcium measurements in guard cells of YC3.6 lines

Ratiometric calcium measurements in guard cells were performed in epidermal strips as previously described³¹. In brief, leaf discs were stuck onto coverglasses using medical adhesive (Hollister) with the lower epidermis facing the glass. All tissues except for the epidermis were gently removed using a razor blade. Strips were incubated in water overnight in a plant growth chamber at 22 °C and in the light for several hours before starting the measurement. Before the measurement, a chamber was formed around the strip using Carolina Observation Gel (Carolina Biological) and filled with 270 μl water. The coverslip was taped onto a platform and mounted onto a Nikon Eclipse Ti inverted microscope. Excitation was performed at a wavelength of 430/24 nm using a blue light LED (LXK2-PB14-Q00, Lumileds) and an ET430/24 \times excitation filter (Chroma). The microscope was equipped with a 89002bs dual band-pass dichroic mirror (Chroma). CFP and YFP emission fluorescence were separated using an optosplit device (Cairn Research) with a T495LPXR dichroic mirror and an ET470/24m filter for CFP and ET535/30m filter for YFP (Chroma). Images were captured with a RETIGA-SRV CCD camera (Qimaging). Recording was performed using Metafluor 7.8.9.0 software (Universal Imaging). Single guard cells were defined as regions-of-interest. Cells were observed for 5 min at 20-s frame intervals, followed by 5 min at 5-s intervals, before flg22 was added to the bath at time point 10 min. Cells which during this 10-min period showed oscillations (so-called spontaneous oscillations) and just continued to do so after the addition of flg22 were excluded from the analysis as it would not be possible to state that the oscillations after the addition of flg22 were caused by the flg22 as they have been observed already before it was added. Flg22 was

added from a 10× stock in MilliQ-H₂O to yield a final concentration of 1 μM. Analysis was performed using Fiji⁵⁵. Ratio values were determined by dividing YFP by CFP intensities.

Oscillations induced by flg22 in guard cells do not show a defined frequency or period, and different cells, also those belonging to the same stomate, are not synchronized³¹. In addition, peaks often do not return to the baseline before the launch of a new spike. This is in contrast to, for example, the very regular Nod factor-induced spiking, where parameters such as period, frequency and number of spikes can easily be determined⁵⁶, or calcium signals induced by stresses such as osmotic or salt treatment, which are characterized by one defined fast-occurring peak, which can easily be described by its height¹⁵. Oscillations induced by flg22 last for around 30 min. Measuring with YC3.6 over this time period results in bleaching of the reporter over time, whereby YFP and CFP differ in their bleaching characteristics, that is, YFP is bleaching faster. This results in a ratio baseline, which often is neither straight nor linear, and therefore the height of a given peak during the measurement—especially if it is one that has not originated from the baseline—cannot easily be determined. For the same reason, just determining the sum of all values to integrate the signal would not be correct. To account for the normally occurring variability in spiking between cells and the chaotic nature of the oscillations, we analysed the area under the curve in the first five minutes after flg22-treatment as parameter, which represents the speed and strength of the first influx of calcium over the plasma membrane in an objective way. For every replicate, the exact time point of addition of flg22 was set as start time and the analysis performed from the start time to the start time +5 min. Wavelet analysis was chosen to account for correct determination of baseline and peaks. The wavelet analysis produces a wave that is centred around 0 with positive and negative peaks, removing the need to define a basal line and instead taking the $y = 0$. Hence, the AUC can be calculated simply using the trapezoid rule. Original curves and a description of how this analysis was performed are available on https://github.com/TeamMacLean/peak_analysis.

Calcium-flux measurements in guard cells

Guard cell preparation.—Net Ca²⁺ fluxes were measured non-invasively using the scanning ion-selective electrodes^{57,58} (SISE) technique with guard cells in isolated epidermal strips. Lower epidermis from 5- to 6-week-old leaves via double-sided adhesive tape were mounted to the recording chamber and incubated in buffer based on 1 mM KCl, 1 mM CaCl₂ and 10 mM MES, pH 6.0 (Bis-Tris propane) overnight. Following adaptation to the stomatal opening pre-stimulus conditions flg22 was added into the bath solution at final concentration of 1 μM.

Electrode preparation, calibration and experimental set-up for ion flux measurements.—The electrodes were pulled from borosilicate glass capillaries without filament (1.0 mm diameter; Science Products) with a vertical puller (Narishige Scientific Instrument Lab). They were baked overnight at 220 °C and silanized with *N,N*-dimethyltrimethylsilylamine (Sigma-Aldrich) for 1 h. Ca²⁺-selective electrodes were backfilled with 500 mM CaCl₂ and tip filled with calcium ionophore I cocktail A (Sigma-Aldrich). Calibration of Ca²⁺-selective electrodes was performed in solutions containing 10, 1 and 0.1 mM CaCl₂. For lanthanum experiments, electrodes were calibrated with a

1 mM lanthanum background. Only electrodes were used that recorded a shift in voltage of approximately 29 mV per pCa unit. The ion selective electrodes were positioned with a Micromanipulator (PatchStar, Scientifica) at approx. 2 μm distance to a guard cell using an inverted microscope (Axiovert 135, Carl Zeiss AG). The electrode was connected via Ag/AgCl half-cells to the head stage of the microelectrode amplifier (custom-built). Electrode was scanning at 10-s intervals over a distance of 29 μm , using a piezo stepper (Luigs & Neumann GmbH). Raw data were acquired with a NI USB 6259 interface (National Instruments), using the custom-built Labview-based software 'Ion flux monitor'⁵⁸. Raw voltage data were converted offline into ion flux data, as described^{57–60}. For reasons of comparability, all measurements were converted with the same settings in Ion flux monitor. A detailed description of the statistical analysis performed is available at https://github.com/TeamMacLean/peak_analysis.

Stomatal aperture assays

Leaf discs (two leaf discs per plant, three plants per line) were taken from 5- to 6-week-old plants grown on soil and incubated in stomatal opening buffer (10 mM MES-KOH pH 6.15, 50 mM KCl, 10 μM CaCl₂ and 0.01% Tween-20) for 2 h in a plant growth cabinet in the light. Subsequently, flg22, AtPep1, ABA or mock were added from stock solutions to the indicated concentrations and samples incubated under the same conditions for another 2–3 h. Photographs of the abaxial leaf surface were taken using a Leica DM5500 microscope equipped with a Leica DFC450 camera. Width and length of the stomatal openings were determined using the Leica LAS AF software and aperture given as ratio of width divided by length.

Number of stomata counted and underlying statistical analysis in Fig. 4 are: Fig. 4b: Col-0 mock: $n = 346$, Col-0 flg22: $n = 381$, *osca1.3* mock: $n = 382$, *osca1.3* flg22: $n = 435$, *osca1.7* mock: $n = 435$, *osca1.7* flg22: $n = 448$, *osca1.3/1.7* mock: $n = 460$, *osca1.3/1.7* flg22: $n = 497$. Figure 4c: Col-0 mock: $n = 410$, Col-0 AtPep1: $n = 546$, Col-0 ABA: $n = 484$, *osca1.3/1.7* mock: $n = 477$, *osca1.3/1.7* AtPep1: $n = 520$, *osca1.3/1.7* ABA: $n = 467$. Figure 4f: Col-0 mock: $n = 154$, Col-0 flg22: $n = 159$, *osca1.3/1.7* mock: $n = 159$, *osca1.3/1.7* flg22: $n = 181$, *osca1.3/1.7/pOSCA1.3:OSCA1.3(S54A)* mock: $n = 170$, *osca1.3/1.7/pOSCA1.3:OSCA1.3(S54A)* flg22: $n = 197$, *osca1.3/1.7/pOSCA1.3:OSCA1.3* (WT) mock: $n = 108$, *osca1.3/1.7/pOSCA1.3:OSCA1.3* (WT) flg22: $n = 155$.

Gas-exchange measurements

Seeds of Col-0 and *osca1.3/1.7* were sown on sterilized soil, and plants were grown in a climate cabinet with the following conditions: day:night cycle of 12:12 h, temperatures of 21:18 °C, photon flux density of 100 $\mu\text{mol m}^{-2} \text{s}^{-1}$, and relative humidity of 60%. After 12–14 days, the seedlings were carefully transferred to new pots and grown for another 2–3 weeks, at the same conditions.

Leaf transpiration was recorded with intact leaves, of which the petioles were excised from the rosette and immediately transferred to distilled water. The petioles were recut twice under water with a razor blade to avoid embolism, and were quickly transferred into small tubes with distilled water and wrapped with parafilm. Leaves were placed inside the

cuvettes of a custom-made gas exchange recording system⁶¹, equipped with two Infra-Red-Gas-Analyzers (IRGA) (LI 7000; Li-Cor). The air stream through the cuvettes was set to 0.96 l min⁻¹ and had a relative humidity of 68% and a CO₂ concentration of 400 ppm. The leaves were illuminated with LEDs (Cree Xlamp CXA2520 LED) at a photon flux density of 80 μmol m⁻² s⁻¹. During the measurements, stimuli were added to the solution at the petioles to concentrations of 10 μM flg22, 3 μM AtPep1, 10 μM ABA or 0.01% ethanol (as a control).

Bacterial spray infection

P. syringae pv. tomato (*Pto*) DC3000 *COR*⁻ strain was grown in overnight culture in King's B medium supplemented with 50 μg ml⁻¹ rifampicin, 50 μg ml⁻¹ kanamycin and 100 μg ml⁻¹ spectinomycin and incubated at 28 °C. Cells were harvested by centrifugation and pellets re-suspended in 10 mM MgCl₂ to an OD₆₀₀ of 0.2, corresponding to 1 × 10⁸ cfu ml⁻¹. Silwet L77 (Sigma Aldrich) was added to a final concentration of 0.04%. Four-to-five-week-old plants (7 to 8 plants per genotype) were sprayed with the suspension and covered with a lid for three days. Three leaf discs were taken from three leaves per plant and ground in 200 μl water using a 2010 Geno/Grinder (SPEXSamplePrep). Serial dilutions of the extracts were plated on L agar medium containing antibiotics and 25 μg ml⁻¹ nystatin. Colonies were counted after incubation at 28 °C for 1.5 to 2 days.

RNA isolation, cDNA and RT-qPCR

For gene-expression analysis, seeds were sown on 0.5×MS medium (2.2 g l⁻¹; including vitamins) supplemented with 1% sucrose and 0.8% agar. Seeds were stratified for 2 days at 4 °C and incubated for 5 days at 21 °C under a 16-h photoperiod. Seedlings were then transferred to liquid 0.5×MS medium with 1% sucrose and grown for another 8 days. Total RNA was extracted from two seedlings using TRI reagent (Ambion) according to the manufacturer's instructions. RNA samples were treated with Turbo DNA-free DNase (Ambion) according to the manufacturer's instructions. RNA was quantified with a Nanodrop spectrophotometer (Thermo Fisher Scientific). cDNA was synthesized from RNA using RevertAid Reverse Transcriptase (Thermo Fisher Scientific) according to the manufacturer's instructions. cDNA was amplified by quantitative PCR using PowerUp SYBR Green Master mix (Thermo Fisher Scientific) and an Applied Biosystems 7500 Fast Real-Time PCR System (Thermo Fisher Scientific). Relative expression values were determined using *U-box* (At5g15400) as a reference and the comparative C_t method (2^{-C_t}). Primers used are listed in Supplementary Table 2.

Statistical analysis

Statistical analysis was performed in GraphPad Prism 7.0. (GraphPad Software, <http://www.graphpad.com>) unless stated otherwise. Dot plots were used to show individual data points wherever possible. *P* values over 0.05 were considered non-significant. Sample sizes, statistical tests used and *P* values are stated in the figure legends.

Reporting summary

Further information on research design is available in the Nature Research Reporting Summary linked to this paper.

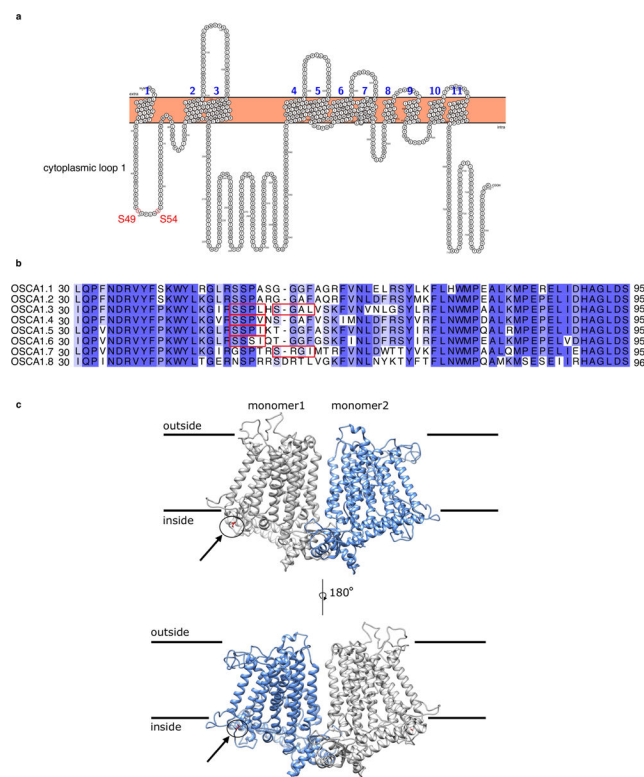
Data availability

Blot source images are presented in Supplementary Fig. 1. Identifiers for publicly available *Arabidopsis* lines are provided in Methods. Raw data and a detailed description of the analysis presented in Fig. 4a have been deposited on GitHub: https://github.com/TeamMacLean/peak_analysis. All SRM assay information and raw data have been deposited to the Panorama Skyline server and can be accessed via <https://panoramaweb.org/Vzao3P.url>. Source data are provided with this paper.

Code availability

All codes used for the wavelet analysis are available at https://github.com/TeamMacLean/peak_analysis.

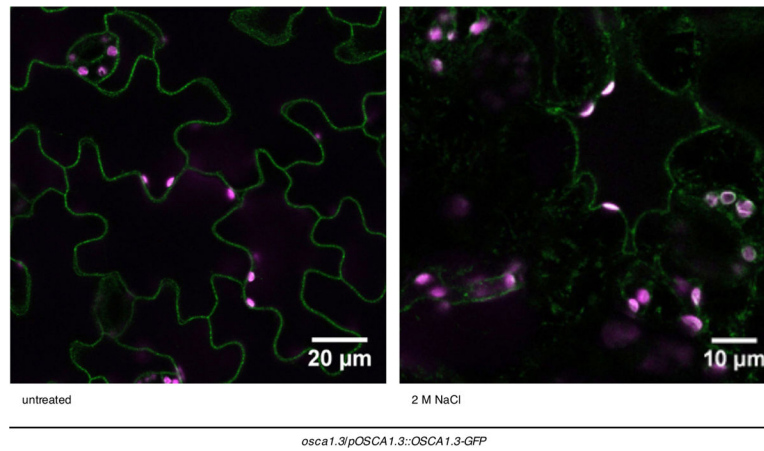
Extended Data



Extended Data Fig. 1 | Predicted topology of OSCA1.3 with possible BIK1 phosphorylation sites and multiple alignment of loop 1 from Clade 1 OSCA proteins.

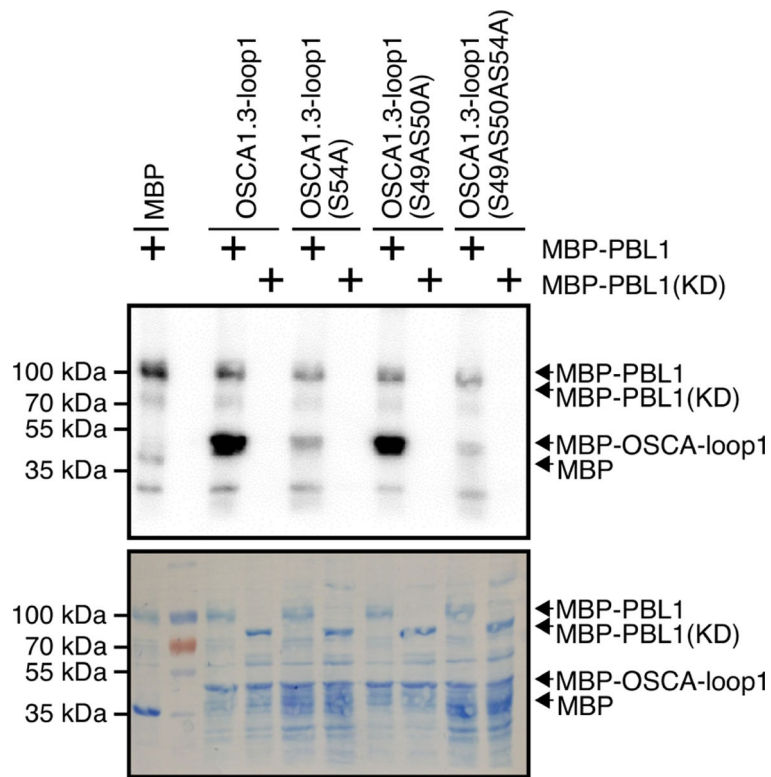
a, Topology was visualized using Protter (www.wlab.ethz.ch/protter) version 1.0 on the basis of information from ref.²⁶. Blue numbers indicate transmembrane regions. Possible BIK1 phosphorylation sites are highlighted in red. **b**, Protein sequence alignment of OSCA1.1 to

OSCA1.8 showing amino acids 30 to 95. Clustal Omega alignments were visualized with Jalview 2.10.5. Possible BIK1 phosphorylation motifs (SxxL/I) are highlighted in red. Blue colour denotes % identity. **c**, Structural model for OSCA1.3. Arrows indicate the position of S54 located in the cytosolic loop.



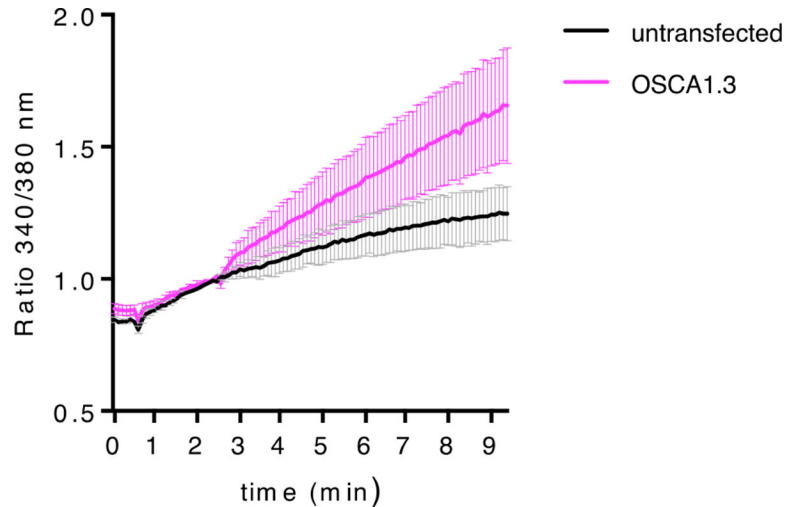
Extended Data Fig. 2 | OSCA1.3 localizes to the plasma membrane.

Confocal microscopy of *osca1.3* cotyledons expressing OSCA1.3-GFP under the control of the *OSCA1.3* promoter. Right Panel: Plasmolysis with 2 M NaCl underlines plasma membrane localization. Green: GFP; magenta: chlorophyll autofluorescence. The experiment was performed once.

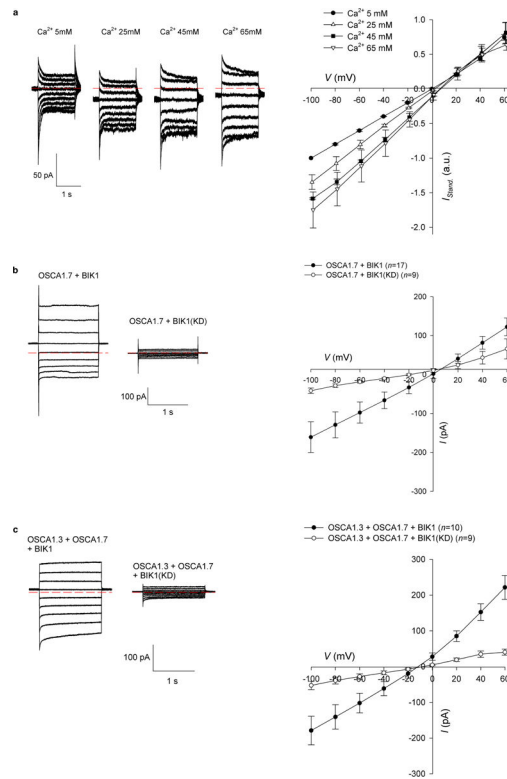


Extended Data Fig. 3 | PBL1 also phosphorylates OSCA1.3.

Differences in PBL1-mediated incorporation of radioactive phosphate in OSCA1.3 and its mutation variants. In vitro kinase assay performed with the corresponding recombinant proteins. For blot source data, see Supplementary Fig. 1. The experiment was performed twice with similar results.

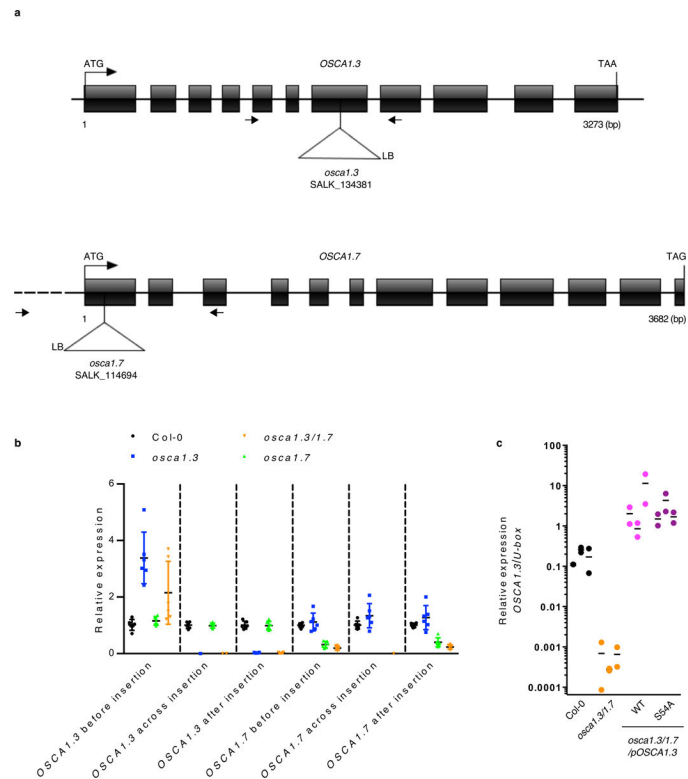
**Extended Data Fig. 4 | OSCA1.3 promotes calcium influx in HEK cells.**

HEK293T cells loaded with the calcium indicator Fura-2 and transfected with OSCA1.3-myc show an increase in fluorescence intensity ratio at 340/380 nm excitation compared to non-transfected cells after addition of sorbitol and calcium to the culture medium, indicating an increase in calcium influx. Data show mean \pm s.d. ($n = 4$ technical replicates). Similar results were obtained in 3 independent biological repeats.



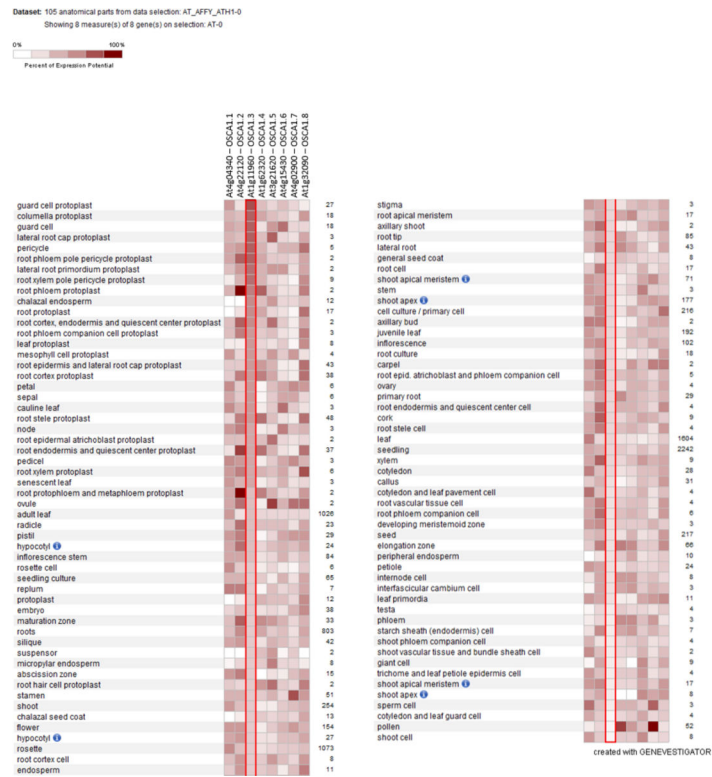
Extended Data Fig. 5 | OSCA1.3 and OSCA1.7 are BIK1-activated calcium-permeable channels.

a, Typical currents (left panel) and corresponding I/V curves (right panel) recorded in OSCA1.3 plus BIK1 expressing COS-7 cells increase with increasing calcium concentrations as indicated on the figure legend ($n = 3$ cells, mean \pm s.e.m.). Currents were normalized with current intensities recorded at -100 mV in the standard bath solution (5 mM calcium), and consequently expressed in normalized arbitrary units for easier comparison of reverse potential changes. Note the inward currents increase and the reverse potentials shift to positive values when extracellular calcium concentration increases, indicating a calcium permeation of the channel. See methods for solutions composition. **b,** Typical traces (left panel) and corresponding statistical analysis (right panel) of currents recorded in whole-cell configuration in COS-7 cells co-transfected with pCI-OSCA1.7 plus pCI-BIK1 ($n = 17$ cells, mean \pm s.e.m.) or plus pCI-BIK1(KD) ($n = 9$ cells, mean \pm s.e.m.) as indicated on the figure legend. OSCA1.7 is a BIK1-activated channel. I/V curves recorded on cells. **c,** BIK1 kinase activity activates currents in cells expressing both OSCA1.3 and OSCA1.7. Typical currents (left panel) and corresponding I/V curves (right panel) recorded in cells co-transfected with both pCI-OSCA1.3 and pCI-OSCA1.7 plus pCI-BIK1 ($n = 10$ cells, mean \pm s.e.m.) or plus pCI-BIK1(KD) ($n = 9$ cells, mean \pm s.e.m.) as indicated on the figure legend. Note that current intensities are not higher than current intensities recorded in cells expressing either OSCA1.3+BIK1 (Fig. 3b, c) or OSCA1.7+BIK1 (**a**), giving no indication on functional heteromerization of OSCA1.3 and OSCA1.7. Whole-cell patch clamp protocols used in b and c were identical to the one used in Fig. 3b, c.

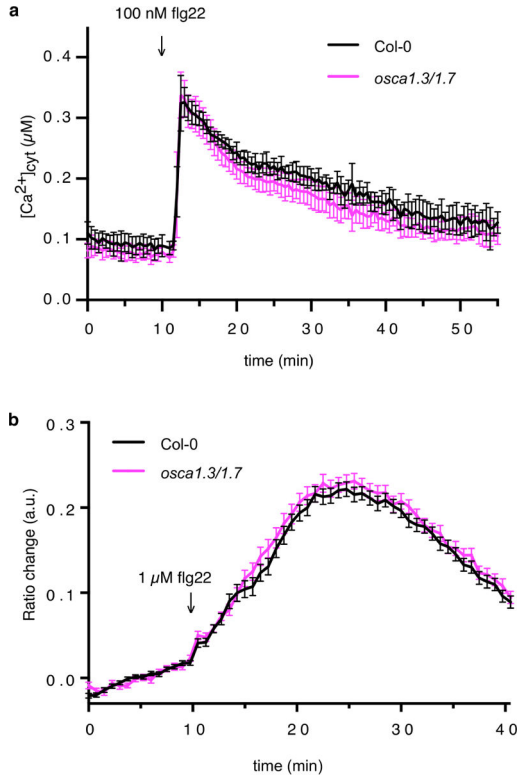


Extended Data Fig. 6 | T-DNA insertion lines used in this study and transcript levels.

a, Gene structure of *OSCA1.3* and *OSCA1.7* showing exons (black boxes) and introns (lines) as well as location of T-DNA insertions. Line *osca1.3/1.7* was obtained by crossing *osca1.3* and *osca1.7*. Arrows denote location of primers used for genotyping. **b**, Transcript levels of *OSCA1.3* and *OSCA1.7* in Col-0, *osca1.3*, *osca1.7* and *osca1.3/1.7* as determined by quantitative real-time PCR with reverse transcription. Values are mean \pm s.d. ($n = 6$, representing 2 independent experiments with 3 biological repeats each). **c**, Transcript levels of *OSCA1.3* in Col-0, *osca1.3/1.7* and *osca1.3/1.7* complemented with *OSCA1.3(WT)* or *OSCA1.3(S54A)*, respectively. Expression levels for three independent T1 plants corresponding to Fig. 4f are shown separately, with two technical replicates (leaves). This experiment was repeated three times. Shown are quantitative real-time RT-PCR data relative to *U-box* (At5g15400). Primers used in **b** and **c** are listed in Supplementary Table 2.

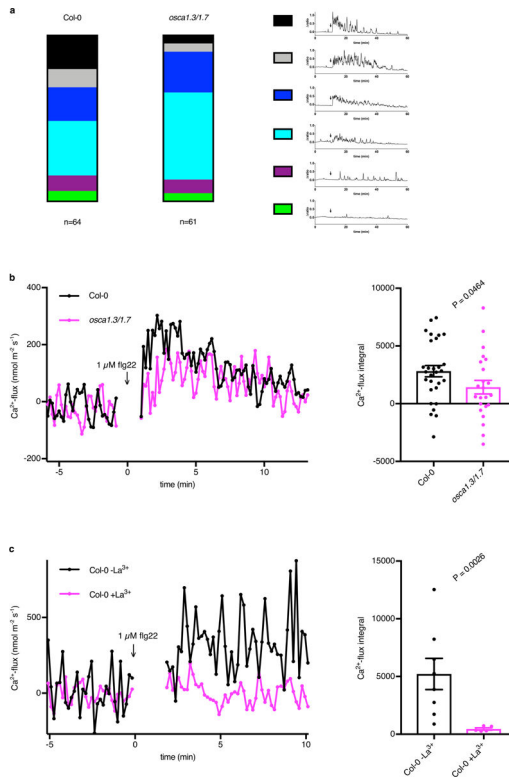


Extended Data Fig. 7 |. Expression pattern of *OSCA* genes from Clade 1. Tissue-specific expression patterns were obtained from Genevestigator (www.genevestigator.com). *OSCA1.3* shows high expression levels in guard cells and guard cell protoplasts.



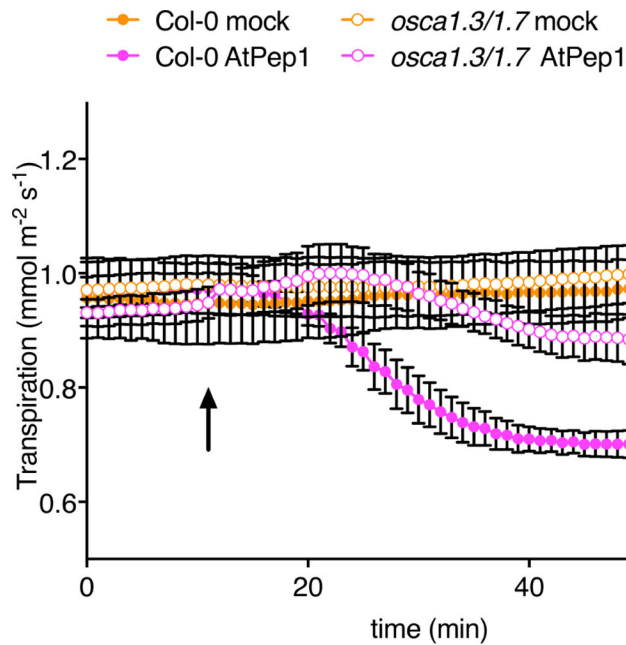
Extended Data Fig. 8 | Fig22-induced calcium influx measured in leaf discs is comparable between wild-type and *osca1.3/1.7* plants.

a. Calcium influx in leaf discs taken of Col-0 and *osca1.3/1.7* plants expressing the calcium reporter aequorin. flg22 was added at time point 10 min. Error bars represent mean \pm s.d. ($n = 12$ leaf discs from 6 independent plants). The experiment was performed twice with similar results. **b.** Average values of FRET ratio changes in leaf discs of Col-0 and *osca1.3/1.7* expressing the ratiometric calcium reporter YC3.6 obtained in plate reader-based assays. Error bars show s.e.m., $n = 90$ leaf discs (Col-0) and 47 leaf discs (*osca1.3/1.7*), with 6 leaf discs taken per individual plant. The experiment was performed twice with similar results.



Extended Data Fig. 9 | Flg22-induced calcium fluxes in *osca1.3/1.7* guard cells are reduced compared to wild-type guard cells.

a, Typical flg22-induced spiking patterns and their distribution in Col-0 and *osca1.3/1.7* guard cells. Legends show ratio changes of the Yellow Cameleon 3.6 calcium reporter observed over time (flg22 added at time point 10 min, indicated by an arrow). The pattern of every cell ($n = 64$ for wild-type and $n = 61$ for *osca1.3/1.7*) was assigned to one of the categories based on visual assessment. **b**, Left panel, net calcium fluxes of a representative Col-0 and *osca1.3/1.7* guard cell, respectively, measured using Scanning Ion Selective Electrodes (SISE). Right panel, integrated calcium fluxes over 7 min after addition of flg22 are reduced in *osca1.3/1.7* compared to Col-0 ($n = 29$ cells for Col-0, $n = 23$ cells for *osca1.3/1.7*; error bars represent mean \pm s.e.m. bootstrapped Welch two sample t -test, two-sided $P = 0.0464$). **c**, Left panel, flg22-induced calcium fluxes are blocked by lanthanum. Representative calcium fluxes measured using Scanning Ion Selective Electrodes (SISE) of Col-0 guard cells with or without lanthanum pre-treatment (1 mM lanthanum applied 10 min before flg22 treatment). One micromolar flg22 was added at time point 0 to epidermal strips. Right panel, integrated calcium fluxes over 8 min after addition of flg22 are significantly blocked by lanthanum in Col-0 ($n = 8$ cells without lanthanum and $n = 5$ cells with lanthanum; error bars represent mean \pm s.e.m.; bootstrapped Welch two sample t -test, two-sided $P = 0.0026$).



Extended Data Fig. 10 | AtPep1-induced decrease in stomatal conductance is impaired in *osca1.3/1.7*.

Leaf transpiration was recorded in excised intact leaves. AtPep1 was added to the solution at the petioles to a concentration of 3 μ M, water was used as control. Data show mean \pm s.e.m. (Col-0 mock, Col-0 AtPep1, *osca1.3/1.7* AtPep1: $n = 8$; *osca1.3/1.7* mock: $n = 11$ leaves).

Supplementary Material

Refer to Web version on PubMed Central for supplementary material.

Acknowledgements

We thank H. Krutinová and S. Vanneste for assistance in early stages of this project; J. P. Kukkonen for assistance for setting up the HEK293T cell assays; J. Sun for assistance with Ca²⁺ measurements in guard cells; B. Brandt for help with structural modelling of OSCA1.3; P. He and E. Peiter for providing published materials; J. -M. Zhou for early strategic discussions on this project and for providing published materials; M. Smoker, J. Taylor and J. Lopez from the TSL Plant Transformation support group for plant transformation; the John Innes Centre Horticultural Services for plant care; and all past and current members of the Zipfel group for technical help and fruitful discussions. This work was supported by the European Research Council under the Grant Agreements No. 309858 and 773153 (grants 'PHOSPHinnATE' and 'IMMUNO-PEPTALK' to C.Z.), The Gatsby Charitable Foundation (to C.Z.), the University of Zürich (to C.Z.), and the Swiss National Science Foundation (grant 31003A_182625 to C.Z.). The Biotechnology and Biological Research Council supported C.Z. and G.E.D.O. with BB/P012574/1. S.J., J.D., T.A.D. and J. Gronnier were supported by post-doctoral fellowships from the European Molecular Biology Organization (EMBO-LTF no. 225-2015; EMBO-LTF no. 683-2018; EMBO-LTF no. 100-2017 and EMBO-LTF no. 438-2018, respectively). Y.K. was supported by JSPS KAKENHI Grant Numbers JP16H06186 and JP16KT0037. Work in the J.F. laboratory was supported by the National Institutes of Health (NIH R01 GM131043), the National Science Foundation (MCB1616437/2016 and MCB1930165/2019) and the University of Maryland. Work in the M.W. laboratory was supported by the Academy of Finland (grant numbers 275632, 283139 and 312498). R.H. and M.R.G.R. were supported by the German Research Foundation (DFG, HE 1640/34-1; HE 1640/40-1; RO2381/6-1 and RO2381/8-1).

References

- Melotto M, Zhang L, Obléssuc PR & He SY Stomatal defense a decade later. *Plant Physiol.* 174, 561–571 (2017). [PubMed: 28341769]

2. Sussmilch FC, Schultz J, Hedrich R & Roelfsema MRG Acquiring control: the evolution of stomatal signalling pathways. *Trends Plant Sci.* 24, 342–351 (2019). [PubMed: 30797685]
3. Hedrich R Ion channels in plants. *Physiol. Rev.* 92, 1777–1811 (2012). [PubMed: 23073631]
4. Jezek M & Blatt MR The membrane transport system of the guard cell and its integration for stomatal dynamics. *Plant Physiol.* 174, 487–519 (2017). [PubMed: 28408539]
5. Berridge MJ, Lipp P & Bootman MD The versatility and universality of calcium signalling. *Nat. Rev. Mol. Cell Biol.* 1, 11–21 (2000). [PubMed: 11413485]
6. Dodd AN, Kudla J & Sanders D The language of calcium signaling. *Annu. Rev. Plant Biol.* 61, 593–620 (2010). [PubMed: 20192754]
7. Kudla J et al. Advances and current challenges in calcium signaling. *New Phytol.* 218, 414–431 (2018). [PubMed: 29332310]
8. Liang X & Zhou J-M Receptor-like cytoplasmic kinases: central players in plant receptor kinase-mediated signaling. *Annu. Rev. Plant Biol.* 69, 267–299 (2018). [PubMed: 29719165]
9. Yu X, Feng B, He P & Shan L From chaos to harmony: responses and signaling upon microbial pattern recognition. *Annu. Rev. Phytopathol.* 55, 109–137 (2017). [PubMed: 28525309]
10. Kadota Y et al. Direct regulation of the NADPH oxidase RBOHD by the PRR-associated kinase BIK1 during plant immunity. *Mol. Cell.* 54, 43–55 (2014). [PubMed: 24630626]
11. Li L et al. The FLS2-associated kinase BIK1 directly phosphorylates the NADPH oxidase RbohD to control plant immunity. *Cell Host Microbe.* 15, 329–338 (2014). [PubMed: 24629339]
12. Ranf S et al. Microbe-associated molecular pattern-induced calcium signaling requires the receptor-like cytoplasmic kinases, PBL1 and BIK1. *BMC Plant Biol.* 14, 374 (2014). [PubMed: 25522736]
13. Monaghan J, Matschi S, Romeis T & Zipfel C The calcium-dependent protein kinase CPK28 negatively regulates the BIK1-mediated PAMP-induced calcium burst. *Plant Signal. Behav.* 10, e1018497 (2015). [PubMed: 26039480]
14. Tian W et al. A calmodulin-gated calcium channel links pathogen patterns to plant immunity. *Nature.* 572, 131–135 (2019). [PubMed: 31316205]
15. Yuan F et al. OSCA1 mediates osmotic-stress-evoked Ca²⁺ increases vital for osmosensing in *Arabidopsis*. *Nature.* 514, 367–371 (2014). [PubMed: 25162526]
16. Hou C et al. DUF221 proteins are a family of osmosensitive calcium-permeable cation channels conserved across eukaryotes. *Cell Res.* 24, 632–635 (2014). [PubMed: 24503647]
17. Li Y et al. Genome-wide survey and expression analysis of the OSCA gene family in rice. *BMC Plant Biol.* 15, 261 (2015). [PubMed: 26503287]
18. Ganie SA, Pani DR & Mondal TK Genome-wide analysis of DUF221 domain-containing gene family in *Oryza* species and identification of its salinity stress-responsive members in rice. *PLoS ONE* 12, e0182469 (2017). [PubMed: 28846681]
19. Ding S, Feng X, Du H & Wang H Genome-wide analysis of maize *OSCA* family members and their involvement in drought stress. *PeerJ* 7, e6765 (2019). [PubMed: 30997296]
20. Benschop J et al. Quantitative phosphoproteomics of early elicitor signaling in *Arabidopsis*. *Mol. Cell. Proteomics.* 6, 1198–1214 (2007). [PubMed: 17317660]
21. Gómez-Gómez L & Boller T FLS2: an LRR receptor-like kinase involved in the perception of the bacterial elicitor flagellin in *Arabidopsis*. *Mol. Cell.* 5, 1003–1011 (2000). [PubMed: 10911994]
22. Zhang J et al. Receptor-like cytoplasmic kinases integrate signaling from multiple plant immune receptors and are targeted by a *Pseudomonas syringae* effector. *Cell Host Microbe.* 7, 290–301 (2010). [PubMed: 20413097]
23. Lu D et al. A receptor-like cytoplasmic kinase, BIK1, associates with a flagellin receptor complex to initiate plant innate immunity. *Proc. Natl Acad. Sci. USA.* 107, 496–501 (2010). [PubMed: 20018686]
24. Murthy S et al. OSCA/TMEM63 are an evolutionarily conserved family of mechanically activated ion channels. *eLife.* 7, e41844 (2018). [PubMed: 30382938]
25. Zhang M et al. Structure of the mechanosensitive OSCA channels. *Nat. Struct. Mol. Biol.* 25, 850–858 (2018). [PubMed: 30190597]
26. Jojoa-Cruz S et al. Cryo-EM structure of the mechanically activated ion channel OSCA1.2. *eLife.* 7, e41845 (2018). [PubMed: 30382939]

27. Liu X, Wang J & Sun L Structure of the hyperosmolality-gated calcium-permeable channel OSCA1.2. *Nat. Commun* 9, 5060 (2018). [PubMed: 30498218]
28. Maity Ket al. Cryo-EM structure of OSCA1.2 from *Oryza sativa* elucidates the mechanical basis of potential membrane hyperosmolality gating. *Proc. Natl Acad. Sci. USA* 116, 14309–14318 (2019). [PubMed: 31227607]
29. Iida H, Nakamura H, Ono T, Okumura MS & Anraku Y *MIDI*, a novel *Saccharomyces cerevisiae* gene encoding a plasma membrane protein, is required for Ca²⁺ influx and mating. *Mol. Cell. Biol* 14, 8259–8271 (1994). [PubMed: 7526155]
30. Knight MR, Campbell AK, Smith SM & Trewavas AJ Transgenic plant aequorin reports the effects of touch and cold-shock and elicitors on cytoplasmic calcium. *Nature* 352, 524–526 (1991). [PubMed: 1865907]
31. Thor K & Peiter E Cytosolic calcium signals elicited by the pathogen-associated molecular pattern flg22 in stomatal guard cells are of an oscillatory nature. *New Phytol.* 204, 873–881 (2014). [PubMed: 25243759]
32. Montillet J-L et al. An abscisic acid-independent oxylipin pathway controls stomatal closure and immune defense in *Arabidopsis*. *PLoS Biol.* 11, e1001513 (2013). [PubMed: 23526882]
33. Liu Yet al. Anion channel SLAH3 is a regulatory target of chitin receptor-associated kinase PBL27 in microbial stomatal closure. *eLife* 8, e44474 (2019). [PubMed: 31524595]
34. Wang Jet al. A cyclic nucleotide-gated channel mediates cytoplasmic calcium elevation and disease resistance in rice. *Cell Res.* 29, 820–831 (2019). [PubMed: 31444468]
35. Kwaaitaal M, Huisman R, Maintz J, Reinstädler A & Panstruga R Ionotropic glutamate receptor (iGluR)-like channels mediate MAMP-induced calcium influx in *Arabidopsis thaliana*. *Biochem. J* 440, 355–373 (2011). [PubMed: 21848515]
36. Ma Y, Walker RK, Zhao Y & Berkowitz GA Linking ligand perception by PEPR pattern recognition receptors to cytosolic Ca²⁺ elevation and downstream immune signaling in plants. *Proc. Natl Acad. Sci. USA* 109, 19852–19857 (2012). [PubMed: 23150556]
37. Espinoza C, Liang Y & Stacey G Chitin receptor CERK1 links salt stress and chitin-triggered innate immunity in *Arabidopsis*. *Plant J.* 89, 984–995 (2017). [PubMed: 27888535]
38. Meena MK et al. The Ca²⁺ channel CNGC19 regulates *Arabidopsis* defense against *Spodoptera* herbivory. *Plant Cell* 31, 1539–1562 (2019). [PubMed: 31076540]
39. Schwessinger Bet al. Phosphorylation-dependent differential regulation of plant growth, cell death, and innate immunity by the regulatory receptor-like kinase BAK1. *PLoS Genet.* 7, e1002046 (2011). [PubMed: 21593986]
40. Cutler SR, Ehrhardt DW, Griffiths JS & Somerville CR Random GFP:cDNA fusions enable visualization of subcellular structures in cells of *Arabidopsis* at a high frequency. *Proc. Natl Acad. Sci. USA* 97, 3718–3723 (2000). [PubMed: 10737809]
41. Waterhouse A et al. SWISS-MODEL: homology modelling of protein structures and complexes. *Nucleic Acids Res.* 46 (W1), W296–W303 (2018). [PubMed: 29788355]
42. Söding J, Biegert A & Lupas AN The HHpred interactive server for protein homology detection and structure prediction. *Nucleic Acids Res.* 33, W244–W248 (2005). [PubMed: 15980461]
43. Pettersen EF et al. UCSF Chimera—a visualization system for exploratory research and analysis. *J. Comput. Chem* 25, 1605–1612 (2004). [PubMed: 15264254]
44. Monaghan Jet al. The calcium-dependent protein kinase CPK28 buffers plant immunity and regulates BIK1 turnover. *Cell Host Microbe* 16, 605–615 (2014). [PubMed: 25525792]
45. Nakagawa Tet al. Development of series of gateway binary vectors, pGWBs, for realizing efficient construction of fusion genes for plant transformation. *J. Biosci. Bioeng* 104, 34–41 (2007). [PubMed: 17697981]
46. Bender KW et al. Autophosphorylation-based calcium (Ca²⁺) sensitivity priming and Ca²⁺/calmodulin inhibition of *Arabidopsis thaliana* Ca²⁺-dependent protein kinase 28 (CPK28). *J. Biol. Chem* 292, 3988–4002 (2017). [PubMed: 28154194]
47. MacLean Bet al. Skyline: an open source document editor for creating and analyzing targeted proteomics experiments. *Bioinformatics* 26, 966–968 (2010). [PubMed: 20147306]
48. Charpentier Met al. Nuclear-localized cyclic nucleotide-gated channels mediate symbiotic calcium oscillations. *Science* 352, 1102–1105 (2016). [PubMed: 27230377]

49. Fischer Met al. The *Saccharomyces cerevisiae* *CCH1* gene is involved in calcium influx and mating. *FEBS Lett.* 419, 259–262 (1997). [PubMed: 9428646]
50. Gietz RD & Woods RA Genetic transformation of yeast. *Biotechniques* 30, 816–831 (2001). [PubMed: 11314265]
51. Reyes Ret al. Cloning and expression of a novel pH-sensitive two pore domain K⁺ channel from human kidney. *J. Biol. Chem* 273, 30863–30869 (1998). [PubMed: 9812978]
52. Jurman ME, Boland LM, Liu Y & Yellen G Visual identification of individual transfected cells for electrophysiology using antibody-coated beads. *Biotechniques* 17, 876–881 (1994). [PubMed: 7840967]
53. Hamill OP, Marty A, Neher E, Sakmann B & Sigworth FJ Improved patch-clamp techniques for high-resolution current recording from cells and cell-free membrane patches. *Pflugers Arch.* 391, 85–100 (1981). [PubMed: 6270629]
54. Moyer C, Hammond-Kosack KE, Jones J, Knight MR & Johannes E Systemin triggers an increase of cytoplasmic calcium in tomato mesophyll cells: Ca²⁺ mobilization from intra- and extracellular compartments. *Plant Cell Environ.* 21, 1101–1111 (1998).
55. Schindelin Jet al. Fiji: an open-source platform for biological-image analysis. *Nat. Methods* 9, 676–682 (2012). [PubMed: 22743772]
56. Miwa H, Sun J, Oldroyd GED & Downie JA Analysis of calcium spiking using a cameleon calcium sensor reveals that nodulation gene expression is regulated by calcium spike number and the developmental status of the cell. *Plant J.* 48, 883–894 (2006). [PubMed: 17227545]
57. Böhm Jet al. Understanding the molecular basis of salt sequestration in epidermal bladder cells of *Chenopodium quinoa*. *Curr. Biol* 28, 3075–3085.e7 (2018). [PubMed: 30245105]
58. Dindas Jet al. AUX1-mediated root hair auxin influx governs SCF^{TIR1/AFB}-type Ca²⁺ signaling. *Nat. Commun* 9, 1174 (2018). [PubMed: 29563504]
59. Newman IA Ion transport in roots: measurement of fluxes using ion-selective microelectrodes to characterize transporter function. *Plant Cell Environ.* 24, 1–14 (2001). [PubMed: 11762438]
60. Arif I, Newman IA & Keenlyside N Proton flux measurements from tissues in buffered solution. *Plant Cell Environ.* 18, 1319–1324 (1995).
61. Müller H Met al. The desert plant *Phoenix dactylifera* closes stomata via nitrate-regulated SLAC1 anion channel. *New Phytol.* 216, 150–162 (2017). [PubMed: 28670699]

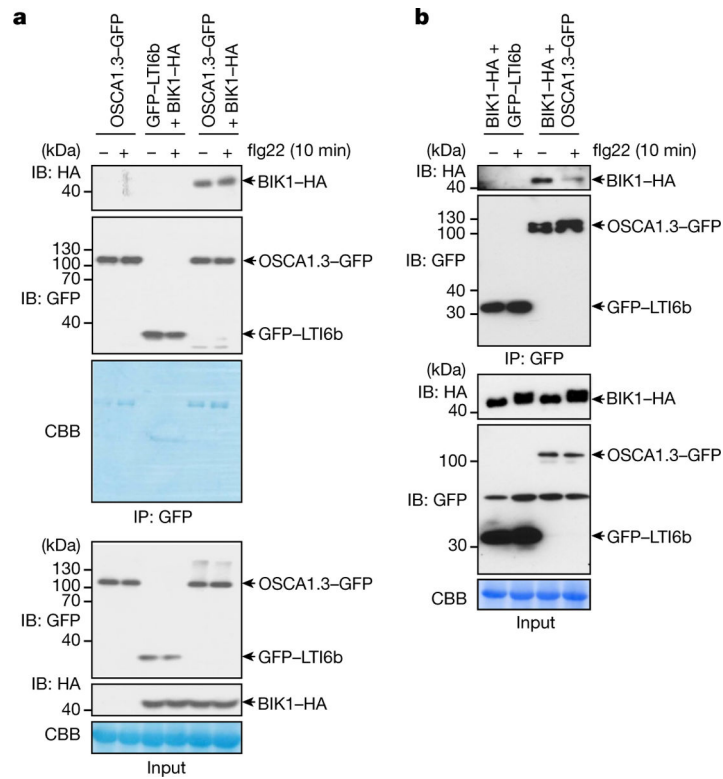


Fig. 1 | OSCA1.3 associates with BIK1.

a, Co-immunoprecipitation of BIK1–haemagglutinin (HA) and OSCA1.3–GFP transiently expressed in *Nicotiana benthamiana* leaves treated with or without 1 μ M flg22 for 10 min. GFP-LTI6b served as negative control. **b**, Co-immunoprecipitation of BIK1–HA and OSCA1.3–GFP from *A. thaliana* lines stably expressing BIK1–HA and OSCA1.3–GFP or GFP–LTI6b, respectively. Immunoprecipitation was performed with GFP agarose beads. Western blots were probed with antibodies against GFP and haemagglutinin. CBB, Coomassie brilliant blue. Uncropped blots are presented in Supplementary Fig. 1. Both experiments were performed three times with similar results.

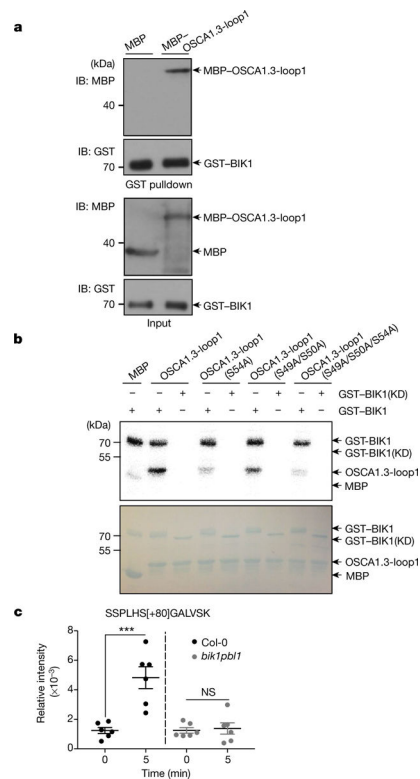


Fig. 2 | OSPA1.3 is phosphorylated by BIK1 and S54 is a major phosphorylation site.

a, In vitro GST pull down with recombinant GST-BIK1 and MBP-OSCA1.3 (amino acids 30–95). MBP was used as control. GST pull down was performed with glutathione resin and western blots probed with GST and MBP antibodies. The experiment was repeated three times with similar results. **b**, In vitro radioactive kinase assay performed with the corresponding recombinant proteins. The experiment was performed three times with similar results. **c** SRM relative quantification of tryptic phosphorylated peptide SSPLHS[+80] GALVSK at 0 and 5 min after flg22 treatment. Values are individual points and mean \pm s.e. ($n = 6$, representing three biological repeats with two technical repeats each). *** $P < 0.0001$ (ordinary one-way ANOVA with multiple comparisons; NS, not significant). Uncropped blots are presented in Supplementary Fig. 1.

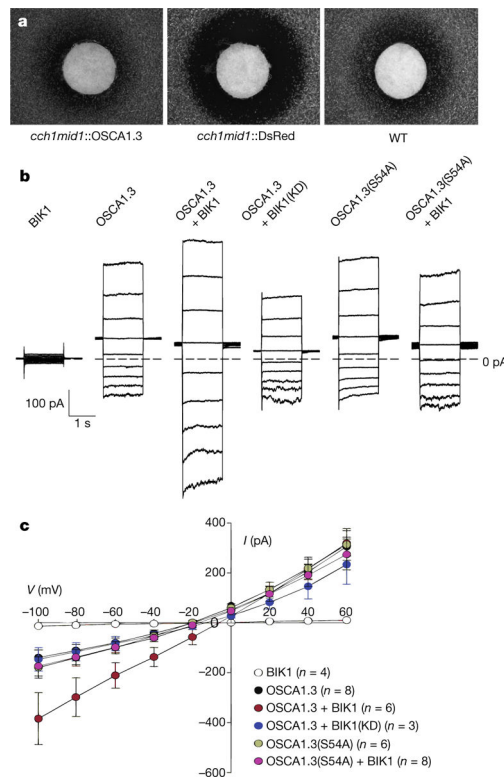


Fig. 3 | OSCA1.3 is a BIK1-activated calcium-permeable channel.

a. OSCA1.3 complements growth of the calcium-uptake-deficient yeast mutant *cch1/mid1*.

Filter discs containing 10 μ g of the mating pheromone α factor were placed on nascent lawns of wild-type (WT) or *cch1/mid1* yeast, or *cch1/mid1* yeast complemented with AtOSCA1.3. DsRed served as control. Photographs were taken after 48 h. OSCA1.3, pYES-DEST52-OSCA1.3, DsRed, pYES-DEST52-DsRed. The experiment was repeated three times with similar results. **b.** Typical currents recorded in whole-cell configuration of COS-7 cells expressing OSCA1.3 or OSCA1.3(S54A) with or without the kinase BIK1 or the mutant BIK1(KD) (BIK1(K105A/K106A)). Voltage pulses were applied from -100 to $+60$ mV (1.5 s long, 20 mV steps). **c.** Current–voltage (I/V) curves of currents shown in **b** ($n > 3$ cells, mean \pm s.e.m.). Solutions had two only main charge carriers, Na^+ and Ca^{2+} , with equilibrium potentials of -66.6 mV (Na^+) and higher than $+60$ mV (Ca^{2+}), respectively. OSCA1.3-mediated currents crossed the x -axis between -10 mV and -20 mV, compatible with the activity of a non-selective cationic channel permeable to Ca^{2+} . Currents recorded at -100 mV in cells expressing OSCA1.3 plus BIK1 were significantly higher than in cells expressing OSCA1.3 alone (one-sided ANOVA, $P = 0.004$).

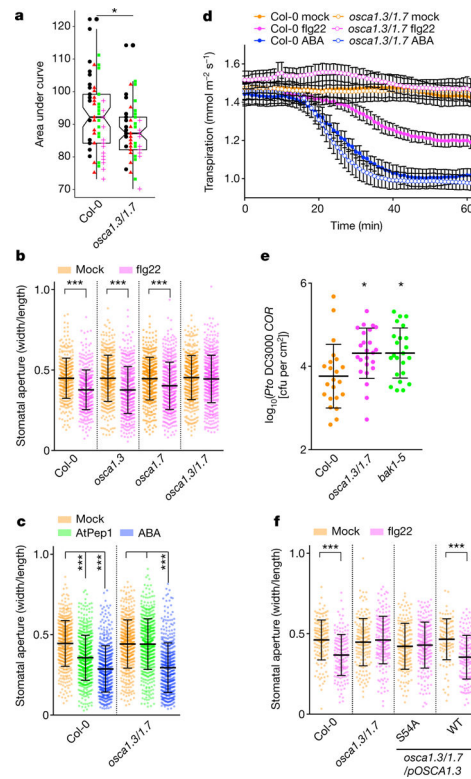


Fig. 4 | OSCA1.3 and OSCA1.7 are required for stomatal immunity.

a, Box and scatter plot showing summed area under the curve (AUC) for wavelet-reconstructed profiles of the first 5 min of flg22-induced calcium spiking in Col-0 YC3.6 and *osca1.3/1.7* YC3.6 guard cells. Each point represents the summed AUC for a single cell. Marker shapes represent individual independent experimental repeats and the box plot represents the distribution of all points for Col-0 or *osca1.3/1.7*. * $P = 0.0024$ ($n = 4$ biological replicates of independently grown batches of plants with three technical replicates and up to six cells assayed; linear mixed-effect model plus ANOVA, one-sided F -distribution). Maxima and minima of scatter are 121 to 72.4, respectively, for Col-0 and 113 to 69, respectively, for *osca1.3/1.7*. In box plots, centre lines show means of 91.6 for Col-0 and 86.7 for *osca1.3/1.7*; hinges are positioned at the 25th and 75th percentiles, and whiskers extend from the hinges to the largest or smallest value no more than $1.5 \times$ the inter-quartile range from the hinge. **b**, Stomatal aperture of wild-type, *osca1.3*, *osca1.7* and *osca1.3/1.7* plants treated with either 5 μM flg22 or water. Individual data points are shown with mean \pm s.d. for $n > 346$ stomata from three experiments. *** $P < 0.0001$ (ordinary one-way ANOVA with multiple comparisons). **c**, Stomatal aperture of wild-type and *osca1.3/1.7* plants treated with water, 5 μM AtPep1 or 10 μM ABA. Individual data points are shown with mean \pm s.d. for $n > 410$ stomata from three experiments. *** $P < 0.0001$ (ordinary one-way ANOVA with multiple comparisons). **d**, Leaf transpiration recorded in excised intact leaves of wild-type and *osca1.3/1.7* plants. Stimuli were added to the solution at the petioles at concentrations of 10 μM flg22 and 10 μM ABA, with 0.01% ethanol as control. Data are mean \pm s.e.m. for $n = 4$ (Col-0 mock, *osca1.3/1.7* flg22 and Col-0 ABA) or $n = 5$ (*osca1.3/1.7* mock, Col-0 flg22 and *osca1.3/1.7* ABA) leaves. The experiment was performed twice with similar results. **e**, Numbers of *P. syringae* pv.

tomato (*Pto*) DC3000 *COR*⁻ bacteria determined 3 days after spray inoculation in Col-0, *osca1.3/1.7* and *bak1-5* plants. Individual data points are shown with mean \pm s.d. for $n = 22$ to 24 plants from three experiments. * $P = 0.012$ (ordinary one-way ANOVA with multiple comparisons). **f**, Stomatal aperture of wild-type, *osca1.3/1.7* plants and *osca1.3/1.7* plants complemented with *pOSCA1.3:OSCA1.3(WT)* or *pOSCA1.3:OSCA1.3(S54A)*, treated with 5 μ M flg22 or water. Individual data points are shown with mean \pm s.d. for $n > 108$ stomata counted over three independent T1 plants. *** $P < 0.0001$ (ordinary one-way ANOVA with multiple comparisons). The experiment was repeated three times with similar results.